

HOT GAS HALOS AROUND DISK GALAXIES: CONFRONTING COSMOLOGICAL SIMULATIONS WITH OBSERVATIONS

JESPER RASMUSSEN,^{1,2} JESPER SOMMER-LARSEN,^{3,4} KRISTIAN PEDERSEN,⁴ SUNE TOFT,⁵ ANDREW BENSON,⁶ RICHARD G. BOWER,⁷ AND LISBETH F. GROVE⁴

Draft version March 4, 2009

ABSTRACT

Models of disk galaxy formation commonly predict the existence of an extended reservoir of accreted hot gas surrounding massive spirals at low redshift. As a test of these models, we use X-ray and H α data of the two massive, quiescent edge-on spirals NGC 5746 and NGC 5170 to investigate the amount and origin of any hot gas in their halos. Contrary to our earlier claim, the *Chandra* analysis of NGC 5746, employing more recent calibration data, does not reveal any significant evidence for diffuse X-ray emission outside the optical disk, with a 3σ upper limit to the halo X-ray luminosity of 4×10^{39} erg s⁻¹. An identical study of the less massive NGC 5170 also fails to detect any extraplanar X-ray emission. By extracting hot halo properties of disk galaxies formed in cosmological hydrodynamical simulations, we compare these results to expectations for cosmological accretion of hot gas by spirals. For Milky Way-sized galaxies, these high-resolution simulations predict hot halo X-ray luminosities which are lower by a factor of ~ 2 compared to our earlier results reported by Toft et al. (2002). We find the new simulation predictions to be consistent with our observational constraints for both NGC 5746 and NGC 5170, while also confirming that the hot gas detected so far around more actively star-forming spirals is in general probably associated with stellar activity in the disk. Observational results on quiescent disk galaxies at the high-mass end are nevertheless providing powerful constraints on theoretical predictions, and hence on the assumed input physics in numerical studies of disk galaxy formation and evolution.

Subject headings: galaxies: formation — galaxies: halos — galaxies: individual (NGC 5170, NGC 5746)
— galaxies: spiral — X-rays: galaxies

1. INTRODUCTION

Estimates of the cosmic baryon fraction, defined as the ratio of baryonic to total mass in the Universe, can be combined with constraints on the integrated mass function of galaxies to infer that most baryons in the Universe are in a hot, diffuse form at the present epoch (Balogh et al. 2001). Cosmological simulations suggest that 30–40 per cent of all baryons reside in intergalactic filaments of shock-heated gas with temperatures $10^5 \lesssim T \lesssim 10^7$ K, the so-called warm/hot intergalactic medium, WHIM (e.g. Cen & Ostriker 1999; Davé et al. 2001). X-ray absorption studies have provided observational evidence for such a component along the line of sight towards a number of quasars (e.g. Tripp et al. 2000; Nicastro et al. 2005; Savage et al. 2005).

While most of the WHIM baryons are predicted to reside in structures of low overdensity, outside the dark matter halos of individual galaxies and groups of galaxies (Davé et al. 2001), a potential repository for some of

the “hidden” baryons in the Universe could be extended halos of hot ($\sim 10^6 - 10^7$ K) gas around individual galaxies, including spirals (e.g. Fukugita & Peebles 2006). For massive galaxies, cosmological simulations suggest that the total mass of these “external” galactic baryons is comparable to that of stars and cold gas in the galaxies themselves (Sommer-Larsen 2006). In a cosmological context, observational support for such a scenario comes from the angular correlations between the galaxy distribution and the soft X-ray background, which indicate the presence of soft X-ray emission from WHIM surrounding individual galaxies (Sothan 2006).

The presence of extended hot gaseous halos around optically bright elliptical galaxies is well established from X-ray observations (e.g. O’Sullivan et al. 2001). The idea that disk galaxies could also be embedded in such halos is integral to many semi-analytical models of disk galaxy formation (e.g., White & Rees 1978; White & Frenk 1991; Cole et al. 2000; Hatton et al. 2003; Bower et al. 2006; Croton et al. 2006). In these models, galaxy dark matter halos are assumed to grow as predicted by spherical infall models, with gas accreting continuously along with the dark matter. During infall into the dark matter potential, the gas is heated, potentially to the halo virial temperature, subsequently cooling radiatively. If cooling is rapid, as is the case for characteristic gas temperatures $T \lesssim 10^6$ K and hence relatively shallow potential wells, no accretion shock develops outside the evolving galactic disk. In these models, present-day spirals of total mass $M \lesssim 10^{11} M_{\odot}$ accrete gas which is predominantly in a cold, non-X-ray emitting phase at temperatures much lower than the virial tem-

¹ Carnegie Observatories, 813 Santa Barbara Street, Pasadena, CA 91101, USA; jr@ociw.edu

² Chandra Fellow

³ Excellence Cluster Universe, Technische Universität München, Boltzmannstr. 2, D-85748 Garching bei München, Germany

⁴ Dark Cosmology Centre, Niels Bohr Institute, University of Copenhagen, Juliane Maries Vej 30, DK-2100 Copenhagen, Denmark

⁵ European Southern Observatory, Karl-Schwarzschild-Str. 2, D-85748 Garching bei München, Germany

⁶ Division of Physics, Mathematics, & Astronomy, California Institute of Technology, Mail Code 130-33, Pasadena, CA 91125, USA

⁷ Institute for Computational Cosmology, University of Durham, South Road, Durham DH1 3LE, UK

perature of their halo (Binney 1977; Birnboim & Dekel 2003; Binney 2004; Kereš et al. 2005; Dekel & Birnboim 2006). This ‘cold accretion’ mode would be particularly pronounced at high redshift, and would imply that most of the halo radiation is emitted as Ly α emission close to the disk. Indeed, observational support for this scenario is accumulating at both low and high redshift (e.g., van der Hulst & Sancisi 2004; Fraternali & Binney 2006; Nilsson et al. 2006; Sancisi et al. 2008; Smith et al. 2008).

At higher galaxy masses and gas temperatures, the gas would emit at X-ray wavelengths but would cool less efficiently, and is then assumed in the models to flow in more slowly than in the fast-cooling regime. A hot X-ray emitting halo can develop, in which the infalling gas is eventually deposited where dictated by its angular momentum. As in the ‘cold accretion’ mode, the gas may ultimately condense to form stars in a rotationally supported disk. In practice, thermal instabilities could act to locally reduce the cooling time of hot halo gas, so in addition to a classical central cooling flow, cooling may also proceed via fragmentation of halo gas into smaller clouds throughout the halo. The net result may be the formation of a multi-phase halo containing warm ($T \sim 10^4$ K), pressure-supported clouds embedded in a large-scale hot corona. These clouds may then rain down onto the disk, possibly akin to some of the high-velocity HI clouds seen around the Galaxy (e.g., Maller & Bullock 2004; Kaufmann et al. 2006; Sommer-Larsen 2006; Peek et al. 2008; but see also Fraternali & Binney 2008). In the scenario proposed by Maller & Bullock (2004), condensation and infall of such clouds would be very important for fueling MW-sized galaxy disks, although at least some numerical work suggests that this mode of accretion is subdominant at $z = 0$ (Sommer-Larsen 2006; Kaufmann et al. 2006; Peek et al. 2008).

The general picture of massive disk galaxies embedded in hot gaseous halos has been backed by cosmological hydrodynamic simulations of galaxy formation (e.g., Toft et al. 2002; Kereš et al. 2005), thus lending support to the general validity of the simplifying assumptions underlying semi-analytical models. For example, the simulations presented by Toft et al. (2002) showed the X-ray luminosity L_X of hot halo gas to scale strongly with disk circular velocity v_c (defined here as the rotation velocity at 2.2 times the disk scale-length; see Sommer-Larsen & Dolgov 2001 for details), with $L_X \propto v_c^{5-7}$, as also expected from semi-analytical models of galaxy formation. It is relevant to note, however, that all the massive galaxies in the Toft et al. (2002) study were formed in the old ‘standard’ ($\Omega_m = 1, \Omega_\Lambda = 0$) cold dark matter cosmology, with a fixed primordial metal abundance and an assumed cosmic baryon fraction well below the currently accepted value. Thus, it seems timely to explore the hot halo predictions of more sophisticated higher-resolution simulations assuming the currently prevailing Λ CDM cosmology. This is one of the goals of this paper.

The existing theoretical results clearly suggest that X-ray observations could provide a useful means of mapping any material accreting onto massive spirals at the present epoch. Direct observational verification of the above scenario has remained elusive, however. In a first study aimed at detecting cosmologically accreted gas halos

around spirals, Benson et al. (2000) compared *ROSAT* X-ray observations of three massive, highly inclined spirals to predictions of simple cooling flow models. The failure of these authors to detect any hot gas around the galaxies translated into upper limits on the halo X-ray luminosity which, for their best-constrained case of NGC 2841, was found to be a factor of 30 below their model prediction. While their models were deliberately simplified versions of general semi-analytical ones, the result persists that some hydrodynamical simulations and simple analytical models overpredict actual halo luminosities (Governato et al. 2004; Benson et al. 2000 and references therein), though the exact magnitude of this discrepancy has yet to be established.

Extended X-ray halos *have* been detected around numerous late-type star-forming spirals (see Strickland et al. 2004a; Tüllmann et al. 2006a and references therein). However, these galaxies typically have at least moderately high star formation rates ($\gtrsim 1 M_\odot \text{ yr}^{-1}$), with the detected halo X-ray emission coinciding with extraplanar H α and radio continuum emission. The standard interpretation is that these multi-phase halos have been generated by star formation activity in the disk, with supernovae expelling hot, X-ray emitting gas, warm and/or photoionized H α -emitting material, and radio synchrotron emitting cosmic ray electrons from the disk (Wang et al. 2001, 2003; Ehle 2004; Strickland et al. 2004a,b; Tüllmann et al. 2006a). Unlike the expectation for gravitationally heated gas, the X-ray luminosity of the gas in the halos of these galaxies is found to correlate with various measures of the disk star formation rate and with the energy input rate by supernovae (SN), but — even when including the diffuse X-ray luminosity of the disk — not with baryonic or HI mass in the disk (Tüllmann et al. 2006b; see also Sun et al. 2007).

Diffuse X-ray emission has also been detected around massive early-type (Sa–Sb) spirals such as NGC 4594 (the ‘Sombrero’ galaxy) (Li et al. 2006, 2007). In these cases, the emission is not obviously associated with star formation in the disk, but the total diffuse X-ray luminosity from the disk and halo still falls well below expectations from cosmological accretion on the basis of the Toft et al. (2002) results. It has been speculated that much of the detected extraplanar emission in these galaxies is heated by SN Ia activity in the disk rather than by gravity (see, e.g., Wang 2007).

Summarizing, the hot halos observed so far around spirals seem to result mainly as a consequence of stellar feedback in the disk rather than infalling intergalactic material. A possible exception is the Milky Way itself, a moderately star-forming galaxy for which indirect arguments can be used to ascertain the presence of an extended reservoir of hot gas possibly related to a gaseous halo (e.g. Moore & Davis 1994; Quilis & Moore 2001; Sembach et al. 2003; Bregman & Lloyd-Davies 2007; Wang 2007). Despite this, it remains unclear whether any of this putative halo gas is actually cooling out to accrete onto the Milky Way disk, and if so, to what extent it can replenish the gas currently being consumed in the disk by star formation.

Sensitive X-ray observations of carefully selected systems are required to settle the question of whether substantial hot gas halos associated with infalling material

exist around quiescent spirals at all. This would provide an important consistency check on the assumptions underlying existing disk galaxy formation models. Motivated by this, we initiated a *Chandra* search for hot X-ray gas surrounding massive, quiescent disk galaxies. As part of this program, the discovery of hot halo gas around NGC 5746, with a total X-ray luminosity of $\sim 4 \times 10^{39}$ erg s $^{-1}$, was reported by Pedersen et al. (2006). In the present paper, we re-visit this issue in more detail using updated *Chandra* calibration data, describe our corresponding *Chandra* results for the less massive galaxy NGC 5170, and present new results from cosmological simulations of galaxy formation and evolution, for direct comparison to the observations. Contrary to the claim in Pedersen et al. (2006), significant extraplanar emission surrounding NGC 5746 is not detected in our updated analysis.

In § 2 we outline our target selection and the analysis of X-ray and optical data. Results for both galaxies are presented in § 3 and compared to predictions of cosmological simulations and to results for generally more actively star-forming spirals in § 4. Some implications of our observational and theoretical results are discussed in § 5, and our findings and conclusions are summarized in § 6. A Hubble constant of $H_0 = 73$ km s $^{-1}$ Mpc $^{-1}$ is assumed throughout. The distances to NGC 5746 and NGC 5170 as listed in NED are then 26.8 and 24.8 Mpc, respectively, with 1 arcmin corresponding to ~ 7.7 and ~ 7.1 kpc. Unless otherwise stated, uncertainties are reported at the 68 per cent confidence level.

2. GALAXY SAMPLE AND DATA ANALYSIS

2.1. Target Selection

The primary objective of this study is to map and characterize any diffuse X-ray gas surrounding quiescent disk galaxies. Our starting point was therefore the simulation results of Toft et al. (2002), in particular the result that halo X-ray luminosity L_X should scale strongly with disk circular velocity v_c . Hence, our target sample was drawn by searching the NED and HyperLeda databases for nearby spiral galaxies with circular velocity $v_c \geq 280$ km s $^{-1}$. According to the results of Toft et al. (2002), this should ensure that the target galaxies are massive enough to generate and retain a large-scale X-ray halo detectable within reasonable *Chandra* exposure times. A further advantage of large v_c lies in the fact that the efficiency with which SN outflows can escape the disk and complicate the interpretation of our results may be expected to decrease with increasing disk mass.

In addition, we required our targets to meet the following criteria: i) inclination $i \geq 80^\circ$, to enable a clean separation between disk and halo gas; ii) distance $D < 40$ Mpc, for similar reasons, and to obtain a sufficiently strong X-ray signal; iii) Galactic latitude $|b| > 30^\circ$, to have a low column density of absorbing foreground Galactic hydrogen, given that any halo emission is expected to be fairly soft and thus subject to significant absorption by intervening material (this criterion excluded a galaxy like NGC 2613, studied by Li et al. 2006); iv) the galaxies should not be a member of a known X-ray bright group or cluster, nor show any significant signs of interaction, so as to include only undisturbed galaxies and avoid significant contamination from hot gas residing

TABLE 1
SALIENT PARAMETERS OF THE OBSERVED DISK GALAXIES

Parameter	NGC 5746	NGC 5170
D (Mpc)	26.8	24.8
RA (J2000)	14 ^h 44 ^m 56 ^s .00	13 ^h 29 ^m 48 ^s .83
Dec (J2000)	+01°57′17″.1	−17°57′59″.4
Hubble type	SBb	Sc
v_c (km s $^{-1}$)	318 ± 10	247 ± 3
D_{25} (arcmin)	(6.92, 1.20)	(8.32, 1.20)
M_B	−21.79	−21.18
M_K	−25.26	−24.35
L_{IR} (L_\odot)	6.2×10^9	3.7×10^9
SFR (M_\odot yr $^{-1}$)	0.9 ± 0.2	0.5 ± 0.1
Inclination	84°	90°
N_{H} (cm $^{-2}$)	3.3×10^{20}	6.9×10^{20}
<i>Chandra</i> obs. ID	3929	3928
<i>Chandra</i> obs. date	2003–04–11	2003–05–18
<i>Chandra</i> exp. (ks)	35.7	31.9

NOTE. — Distances, positions, and magnitudes taken from the NASA/IPAC Extragalactic Database (NED). Disk circular velocity v_c , D_{25} (major and minor diameter of the ellipse outlining a B -band isophotal level of 25 mag arcsec $^{-2}$), and inclination from the HyperLeda database. L_{IR} is the total (8–1000 μm) infrared luminosity, based on *IRAS* fluxes and the relation of Sanders & Mirabel (1996), and SFR the estimated star formation rates (see text for details). Absorbing column density N_{H} is the Galactic value from Dickey & Lockman (1990).

in an ambient intragroup/-cluster medium; v) in order to also minimize contamination from outflows of hot gas, the galaxies should be relatively quiescent, i.e. not show evidence for significant activity related to a starburst or an active galactic nucleus (AGN). This excluded galaxies such as NGC 891, which displays extraplanar X-ray, H α , and radio emission associated with stellar feedback activity (see Temple et al. 2005 and references therein), and the strongly bulge-dominated Seyfert NGC 4594 (the ‘Sombrero’), which hosts a $\sim 10^9 M_\odot$ low-luminosity AGN (Fabbiano & Juda 1997; Bendo et al. 2006).

Imposing these strict criteria, only one galaxy remained, NGC 5746. We therefore relaxed the requirement on v_c to include a second target, NGC 5170, which, although still massive, could act as a consistency check on our analysis procedure. NGC 5746 is an SBb spiral with a circular velocity $v_c = 318 \pm 10$ km s $^{-1}$ (HyperLeda database), and NGC 5170 an Sc spiral with a significantly lower v_c of 247 ± 3 km s $^{-1}$ (Kregel et al. 2004). We note that our selection was not restricted to particular Hubble types, but given the $v_c \geq 280$ km s $^{-1}$ criterion, the selection method is likely to bias against late-type spirals. Since such galaxies are likely to display higher star formation activity at present than early-type ones, this criterion is in turn likely to favor relatively quiescent spirals, as desired. Salient parameters of the observed galaxies are listed in Table 1.

As the goal of this study is to constrain the amount of *infalling* hot halo gas, the requirement of low levels of disk activity is particularly important for ensuring minimal contamination of the extraplanar X-ray flux from *outflowing* hot gas. In terms of their star formation rate (SFR), both galaxies are indeed fairly quiescent, as already evidenced by the fact that none of them is included in the revised catalog of bright *IRAS* galaxies (Sanders et al. 2003), despite their close proximity

and large mass. Their *IRAS* 60 and 100 μm fluxes S_{60} and S_{100} , taken from Moshir et al. (1990) for NGC 5746 and Rice et al. (1988) for NGC 5170, translate into global SFRs of 0.9 ± 0.2 (NGC 5746) and $0.5 \pm 0.1 M_{\odot} \text{ yr}^{-1}$ (NGC 5170), using the relations of Sanders & Mirabel (1996) and Kennicutt (1998). This is equivalent to specific (area-normalized) SFRs of $\sim 4 \times 10^{-4}$ (NGC 5746) and $\sim 2 \times 10^{-4} M_{\odot} \text{ yr}^{-1} \text{ kpc}^{-2}$ (NGC 5170), assuming a circular disk of radius equal to the semi-major axis of D_{25} . For comparison, the moderately quiescent Milky-Way disk displays an SFR of $\sim 2 M_{\odot} \text{ yr}^{-1}$ (see e.g. Casuso & Beckman 2004), corresponding to $\sim 3 \times 10^{-3} M_{\odot} \text{ yr}^{-1} \text{ kpc}^{-2}$. Both galaxies furthermore display low far-infrared ‘temperatures’ of $S_{60}/S_{100} \approx 0.15$ (NGC 5746) and 0.22 (NGC 5170), and their far-infrared luminosities L_{FIR} imply ‘mass-normalized’ star formation rates $L_{\text{FIR}}/L_{\text{B}} \approx 0.06$, further indicative of low star formation activity (see e.g. Read & Ponman 2001 for details).

From a *Chandra* study of extraplanar X-ray emission around nearby disk galaxies covering a range of morphologies and star formation rates, Strickland et al. (2004b) derived a criterion for gas blow-out by supernovae based on the observed properties of the interstellar medium in typical spirals. They find on theoretical grounds that in order to have a collection of near-simultaneous SN expel gas from the disk, the requirement $F_{\text{SN,FIR},D_{25}} \gtrsim 25 \text{ SN Myr}^{-1} \text{ kpc}^{-2}$ must be satisfied. In their notation, $F_{\text{SN,FIR},D_{25}}$ is the rate $\mathcal{R}_{\text{SN}} = 0.2L_{\text{IR}}/10^{11} L_{\odot}$ of core-collapse SN per disk ‘area’ D_{25}^2 . Indeed, for the eight out of ten spirals in their sample with detected extraplanar X-ray emission, they find $F_{\text{SN,FIR},D_{25}} \gtrsim 40 \text{ SN Myr}^{-1} \text{ kpc}^{-2}$. Figure 1 compares the core-collapse SN rates of the galaxies in the Strickland et al. (2004a,b) sample to those inferred for our target galaxies using the same methods. The additional galaxies of Tüllmann et al. (2006a) from a comparable *XMM-Newton* study have also been plotted. Both our targets clearly lie in a regime in which ejection of detectable hot gas by SN would not be anticipated. While these results neglect the contribution from type Ia SNe, low specific SN Ia rates of ≈ 4.7 (NGC 5746) and $3.3 \text{ SN Myr}^{-1} \text{ kpc}^{-2}$ (NGC 5170) can be estimated, using the prescription adopted by Mannucci et al. (2005) and the *K*- and *B*-band magnitudes listed in Table 1. Adding these to the results in Fig. 1 clearly still places both galaxies well below the blowout criterion derived by Strickland et al. (2004b). These results suggest that any extraplanar emission surrounding our targets will be largely uncontaminated by emission from supernova-driven outflows of hot gas, enabling reliable constraints on the physical properties of any accreting material.

2.2. Observations and Analysis

Both disk galaxies were observed by *Chandra* with the ACIS-I array as aimpoint and with the CCD’s at a temperature of -120° C . Data were telemetered in Very Faint mode which allows for superior background suppression relative to standard Faint mode. To exploit this, the data were reprocessed and background screened using CIAO v3.4 with CALDB 3.4.1. Bad pixels were screened out using the bad pixel map provided by the reduction pipeline, and remaining events were grade filtered, excluding *ASCA* grades 1, 5, and 7. Periods of

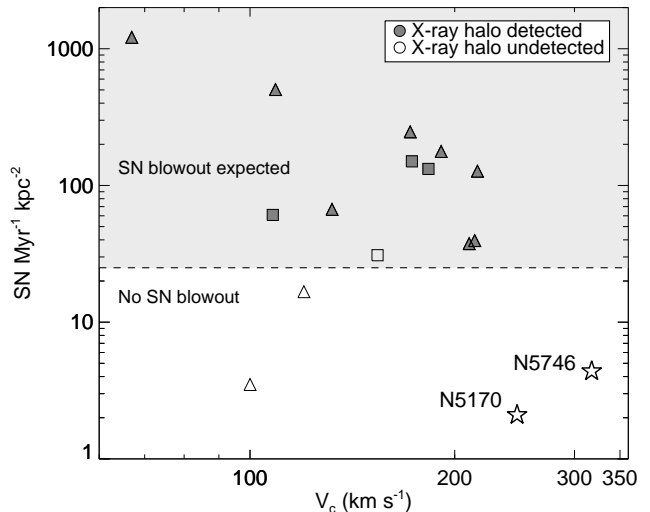


FIG. 1.— Comparison of the specific core-collapse SN rates estimated for our target galaxies (stars) to those in the disk galaxy sample of Strickland et al. (2004a,b) (triangles) and Tüllmann et al. (2006a) (squares). Galaxies with detected extraplanar X-ray emission (in all cases attributed to stellar feedback) are represented by filled symbols. The dashed line marks the expected critical SN rate, $\sim 25 \text{ SN Myr}^{-1} \text{ kpc}^{-2}$, above which SN are expectedly capable of expelling gas from the disk.

high background on the ACIS-I chips were filtered using 3σ clipping of the 0.3–12 keV lightcurves extracted in off-source regions in 259-s bins. Resulting lightcurves showed no strong flaring periods, leaving a total of 35.7 ks (NGC 5746) and 31.9 ks (NGC 5170) of cleaned exposure time.

Point source searches were carried out with the CIAO task ‘wavdetect’ using a range of scales and detection thresholds, and results were combined. A total of 126 (NGC 5746) and 111 (NGC 5170) point sources were detected in the two observations, of which 20 and 17 sources, respectively, are located inside the D_{25} ellipses. Point source extents were quantified using the 4σ detection ellipses from ‘wavdetect’, and these regions were masked out in the analysis of diffuse emission. Further details of the X-ray analysis are described below.

In addition to the X-ray data, we also obtained $\text{H}\alpha$ images of both galaxies with the Danish 1.54-m telescope at La Silla, Chile, for total exposures of 120 (NGC 5746) and 160 min (NGC 5170). In both cases, 20 min *R*-band images were also taken for subsequent continuum-subtraction. The frames were bias-subtracted, flat-fielded, and median-combined using standard IRAF procedures. Using the *R*-band image of each galaxy, we estimated and subtracted the continuum emission contribution to the $\text{H}\alpha$ image as follows. The two combined images were normalized to the same exposure time, and the *R*-band image was smoothed with a Gaussian kernel to match the broader point spread function of the $\text{H}\alpha$ image. The smoothed *R*-band image was then scaled to match the narrower width of the $\text{H}\alpha$ filter and subtracted from the $\text{H}\alpha$ image. For NGC 5746, the background in the resulting continuum-subtracted $\text{H}\alpha$ image had a large-scale gradient caused by stray light from a star just outside the field of view. We modeled this using the SEXTRACTOR software (Bertin & Arnouts 1996)

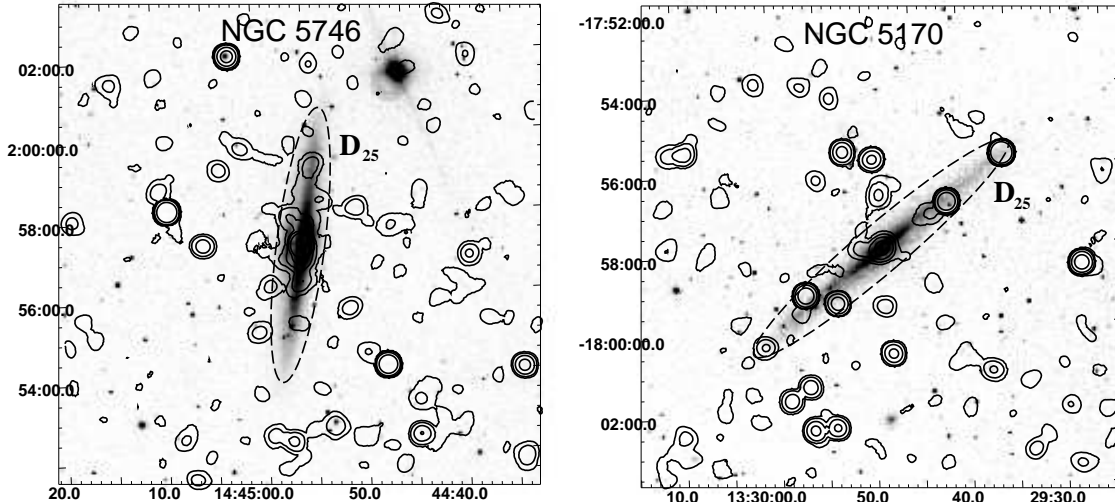


FIG. 2.— 0.3–2 keV exposure-corrected X-ray contours overlaid on our $H\alpha$ images of both galaxies. Contours have been smoothed with a Gaussian of width $\sigma = 20''$, and are logarithmically spaced over a decade beginning at 1.5 times the background level. The D_{25} ellipse is outlined by a dashed contour in each case.

with options set to save a full resolution interpolated background map. Parameters were optimized to generate a map sufficiently fine to represent large scale variations, and sufficiently coarse so as not to include local non-background structures (such as an $H\alpha$ halo around the galaxy). The resulting background map was then subtracted from the $H\alpha$ image.

3. RESULTS

3.1. X-ray and $H\alpha$ Emission

In order to aid the search for diffuse X-ray emission around either galaxy, smoothed, exposure-corrected 0.3–2 keV images were created for both using two separate methods. One involved smoothing the images with a simple Gaussian kernel, while in the other we generated background-subtracted images following the procedure outlined in Rasmussen et al. (2006). In either case, the resulting images were exposure-corrected using similarly smoothed exposure maps. The overall impression conveyed by these images is qualitatively similar, suggesting very little diffuse emission beyond the optical disk of either galaxy. Given the expected weakness of any halo signal, we here only discuss the simple Gaussian smoothed images, so as to accommodate any concerns that adaptive smoothing may introduce spurious features for these low-S/N data. Fig. 2 shows our $H\alpha$ images of the central 12×12 arcmin region around each galaxy, with the Gaussian smoothed X-ray contours overlaid, and with the optical extent of the galaxies outlined by their respective D_{25} ellipses. Clearly, both diffuse and point-like X-ray emission is detected within the optical disks of both galaxies, but there is no immediate indication of any diffuse X-ray or $H\alpha$ emission extending well beyond the disks.

In order to perform a more quantitative search for diffuse X-ray emission around the galaxies, and confirm the overall impression conveyed by Fig. 2, we generated 0.3–2 keV surface brightness profiles of the unsmoothed, exposure-corrected emission. Point sources, chip gaps,

and emission inside D_{25} were masked out. Radial profiles extracted within $r = 40$ kpc ($r \approx 5$ arcmin for NGC 5746) are shown in Figure 3, binned into ten equal-sized radial bins for improved S/N, and with the background level in the data evaluated from a surrounding ($r = 5.5$ – 7.5 arcmin) point source-excised annulus.

These profiles support the conclusion that no significant detectable X-ray emission surrounds either galaxy on large scales. We confirmed that this result does not depend on the specific choice of radial binning scheme. While the NGC 5170 profile shows emission outside D_{25} which is everywhere consistent with a constant level equal to the estimated mean background level, the profile for NGC 5746 does show some deviations from a uniform level. Excess emission is detected in the radial bin immediately outside the optical disk at 2.2σ significance, suggesting the presence of faint extraplanar emission at ~ 5 – 10 kpc from the galactic center. We investigate this in more detail in the inset in Fig. 3a, which displays the NGC 5746 profile extracted in bins perpendicular to the disk. This plot confirms that the excess is not an artifact of the adopted binning scheme, while also indicating that the excess may be largely confined to the eastern side of the disk. However, since the signal is only nominally significant at the $\sim 2\sigma$ level and is comprised of only 15 net photons, we do not consider it robust evidence of diffuse halo emission associated with NGC 5746. It is also worth remarking that a comparably significant *deficit* of emission is seen at larger radii ($r \approx 3.5$ – 4 arcmin), suggesting that the excess may be a spurious feature introduced by local fluctuations in the background level, perhaps caused by the presence of point sources just below our detection limit.

Inside the circular aperture underlying Fig. 3, i.e. with the D_{25} ellipse excluded, we detect a total of 38 net photons in 0.3–2 keV for NGC 5746, corresponding to emission at just 0.8σ above the background. The corresponding result for NGC 5170 shows a *deficit* of 101 photons (significant at 2.1σ) relative to the surrounding background. Qualitatively similar results are obtained in

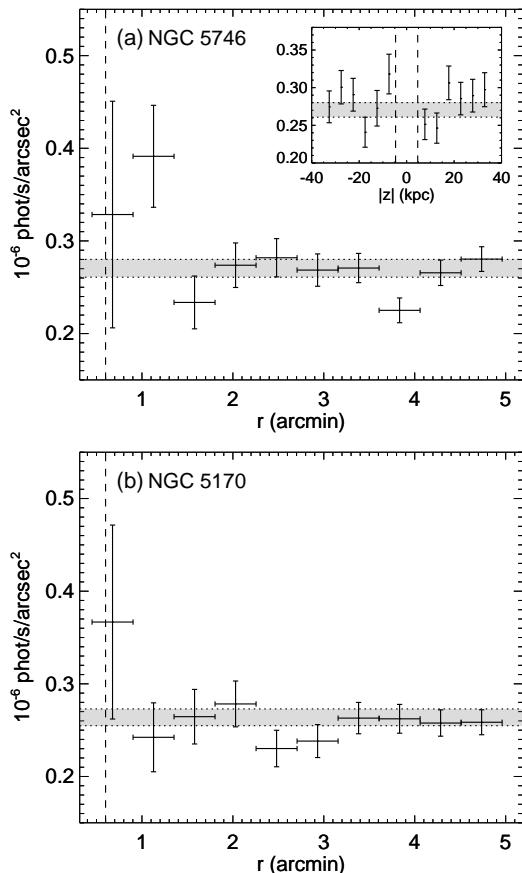


FIG. 3.— 0.3–2 keV exposure-corrected radial surface brightness profiles of (a) NGC 5746 and (b) NGC 5170. Dashed vertical lines outline the maximum extent of the D_{25} ellipse minor axis, and shaded regions mark the 90% confidence uncertainties on the local background level. Point sources, chip gaps, and emission within the D_{25} ellipse itself have been masked out. Inset in (a) shows the NGC 5746 profile (same units, with east to the left) extracted perpendicular to the disk, with D_{25} again masked out.

narrower energy bands such as 0.5–1.5 keV, in which the number of source photons is obviously lower but the ACIS-I S/N from any absorbed $T \sim 0.2$ –0.3 keV plasma should be higher. Hence, the immediate conclusion is that no statistically significant diffuse X-ray emission is detected outside the optical disk of either galaxy on these scales.

In other cases where diffuse X-ray emission has been reported around spirals, this emission is typically accompanied by extended H α and radio halos, with similar overall morphologies (e.g., Strickland et al. 2004a; Tüllmann et al. 2006a). Although there is no indication in Fig. 2 of significant extraplanar H α emission around NGC 5746, we investigate this possibility in more detail in Fig. 4, where we show the surface brightness profile of the H α emission perpendicular to the disk of this galaxy. As can be seen, there is no evidence for significant amounts of H α gas outside the optical extent of the disk. Note that the dip in the H α profile 10 arcsec east of the D_{25} center is due to a dust lane also visible in broadband optical images. For NGC 5170, a similar study has been performed by Rossa & Dettmar (2000), who find no evidence for extraplanar diffuse H α emission surrounding

this galaxy in an H α exposure of similar depth to ours. There is also no indication of significant extraplanar radio emission around either galaxy in the public NRAO VLA Sky Survey (NVSS) 1.4 GHz data of Condon et al. (1998). For NGC 5746, this conclusion is further supported by the NVSS flux density profile extracted from these data, as shown in Fig. 4b. These results provide further testimony to the low star formation activity of both our galaxies, and support the assumption based on Fig. 1 that our constraints on X-ray emission associated with any gas accreting onto these galaxies are not subject to serious contamination by emission from disk outflows.

3.2. Differences with Respect to Pedersen et al. (2006)

The absence of significant detectable diffuse emission around NGC 5746 contrasts with the earlier result of Pedersen et al. (2006) in which a 4σ detection of halo emission was claimed, with a 0.3–2 keV luminosity $L_X = 4.4^{+3.0}_{-1.5} \times 10^{39}$ erg s $^{-1}$ and a plasma temperature of $T = 0.56^{+0.18}_{-0.20}$ keV. Although the modest significance of the detection renders this result tentative rather than conclusive, the difference with respect to our present conclusion demands an attempt at an explanation. We speculate that this discrepancy arises due to a change in the calibration of the time-dependent degradation of the low-energy ACIS CCD quantum efficiency, a possibility also advocated by Wang (2007). This degradation is believed to be caused by a build-up of molecular ice on the *Chandra*/ACIS optical blocking filters or CCD’s¹, an effect which was known but still not well understood at the time of our original analysis in Pedersen et al. (2006).

The properties of the contaminant has remained the focus of continued measurements and is considerably better understood at present. In particular, a model of the *spatial* dependence of the contaminant was introduced with the calibration data in CALDB v. 3.0. However, the analysis of Pedersen et al. (2006) was performed using CALDB v. 2.26, with which the contamination could only be appropriately corrected for in the case of an on-axis source. As contamination is observed to increase towards the edges of the ACIS array, not correctly accounting for this spatial variation will introduce a spurious signal in exposure-corrected low-energy ACIS-I images, appearing as faint diffuse emission whose surface brightness decreases with distance from the CCD aimpoint. It will also lead one to underestimate the soft X-ray background at large off-axis angles.

We conducted a few tests to explore whether this effect could account for the halo signal detected by Pedersen et al. (2006). At a photon energy $E = 0.7$ keV, close to the flux peak energy of a $T \approx 0.6$ keV thermal plasma (the halo temperature inferred by Pedersen et al. 2006), the additional optical depth towards the edges of the CCD arrays can be 0.3–0.5 for data taken around the time of our observations (see previous footnote), implying an apparent reduction in surface brightness at large off-axis angles to 60–75% of the on-axis value. The best-fit (halo plus background) surface brightness model reported by Pedersen et al. (2006) in fact declines at large distances from the NGC 5746 disk to about 75% of the value seen immediately outside the optical disk

¹ http://cxc.harvard.edu/cal/Acis/Cal_prods/qeDeg/

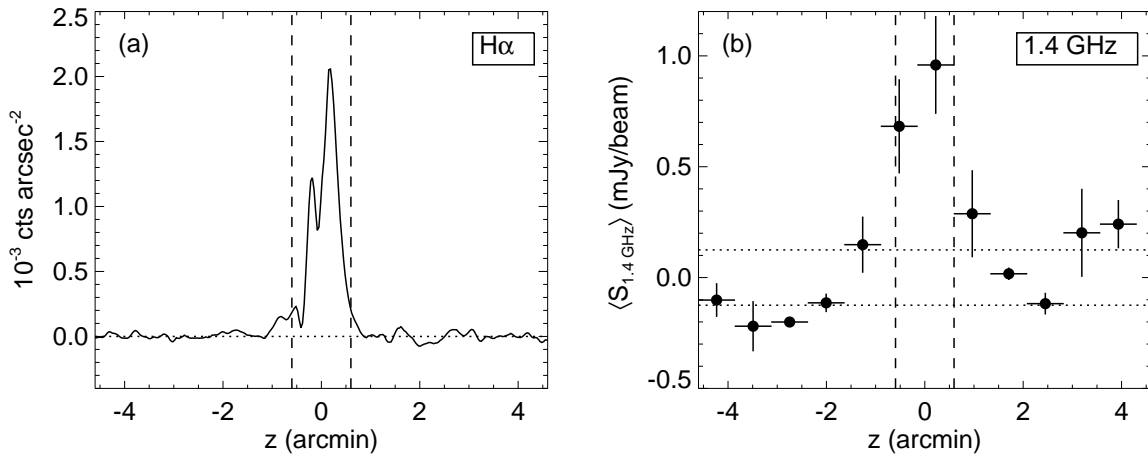


FIG. 4.— (a) Continuum-subtracted $H\alpha$ surface brightness profile of NGC 5746, extracted perpendicular to the disk within the same aperture as that underlying the inset in Fig. 3a (again with east to the left). Bright stars have been masked out. (b) Corresponding mean flux density of 1.4 GHz continuum emission within the same aperture, in bins corresponding to the VLA beam size of 45 arcsec (FWHM). Bright point sources have been masked out. Uncertainties represent the standard deviation within each bin, and dotted lines outline the 1σ errors on the noise level. Dashed vertical lines are as in Fig. 3.

(at $|z| \approx 1.5'$), consistent with the expectation for the spatial variation of the contaminant.

As a further test of this hypothesis, we re-consider the spectral analysis described by Pedersen et al. (2006), in which a double-subtraction approach was employed for the extraction of a background spectrum. This involves extracting a background spectrum for the same detector region as the source region, using blank-sky background data prepared in a similar manner to the source data. This procedure is then repeated for a large-radius annulus, in order to obtain a residual background spectrum that helps to account for any difference in soft X-ray background between source- and blank-sky data. This residual spectrum is then added to the source-region blank-sky spectrum to produce a composite background spectrum. We here repeated the exact same procedure as in Pedersen et al. (2006), while employing the more recent calibration files included with CALDB 3.4.1. In order to mimic the effect of underestimating the soft X-ray background at large radii, as implied by our hypothesis, the normalization of the soft residual spectrum was artificially scaled down so as to achieve ~ 200 net counts in the source region as reported by Pedersen et al. (2006). The resulting background-subtracted source spectrum was then fitted precisely as in our original analysis, yielding a best-fit temperature and unabsorbed 0.3–2 keV luminosity of $T = 0.56_{-0.15}^{+0.19}$ keV and $L_X = 4.0_{-1.2}^{+1.5} \times 10^{39}$ erg s $^{-1}$, respectively, with $\chi^2 = 7.1$ for 9 degrees of freedom. These values are strikingly similar to those obtained by Pedersen et al. (2006).

In summary, both the spatial and spectral properties of the diffuse X-ray halo around NGC 5746 reported by Pedersen et al. (2006) are consistent with the hypothesis that the apparent halo signal was an instrumental artifact caused by the spatial variation in the degradation of the low-energy ACIS quantum efficiency, an effect which our original analysis could not take into account.

The question then arises as to why this calibration problem did not lead to a similar spurious detection of a hot halo around NGC 5170, given that the two galaxies were observed with ACIS-I within one month of each

other and with comparable exposure times. The low signal-to-noise ratio outside the disk in both data sets, including that of the original halo “detection” around NGC 5746, precludes robust conclusions in this regard however, so we can only offer some general considerations. We note that we find no statistically significant differences in the background level between the two data sets in any of a dozen different energy bands or large-radius background regions considered, so global background differences are unlikely to play a major role. The slightly different data preparation criteria applied in our updated analysis could have some impact though, changes in the calibration data aside. For example, our lightcurve screening employs somewhat larger time bins, and has removed a previously undetected minor flare at the end of the NGC 5170 observation. Our current point source search is also slightly more sophisticated, and has resulted in the identification of ten additional point-like sources in the NGC 5170 data (but none such for NGC 5746), of which seven are outside the disk. In combination with the slightly shorter exposure time obtained for NGC 5170, these issues may have played a role in suppressing any faint spurious signal that could mimic diffuse X-ray emission around this galaxy. In addition, we cannot exclude the possibility that the spurious halo signal around NGC 5746 had an additional contribution not present in the NGC 5170 data, e.g. from faint unresolved sources, such as the one hinted at immediately east of the NGC 5746 disk in Figs. 2 and 3a.

3.3. Constraints on Halo Gas Properties

Based on the absence of detectable extraplanar emission around either of our targets, we can constrain some basic properties of any hot halo gas surrounding these galaxies. In this context, it is important not to confuse the signature of cooling halo gas with X-ray emission related to processes in the disk, such as the integrated emission from unresolved discrete sources and from hot gas heated by supernovae and stellar winds. The optical disk of either galaxy is thus excluded in the following analysis. On the other hand, the apparent absence of significant X-ray, $H\alpha$, or radio emission outside the opti-

TABLE 2
DERIVED CONSTRAINTS ON HOT HALO GAS

Galaxy	T (keV)	Z (Z_{\odot})	L_X (erg s^{-1})	$\langle n_e \rangle$ (cm^{-3})	M_{hot} (M_{\odot})	$\langle t_{\text{cool}} \rangle$ (Gyr)	$\langle \dot{M} \rangle$ ($M_{\odot} \text{ yr}^{-1}$)
NGC 5746	0.3 (fixed)	0.2 (fixed)	$< 4.0 \times 10^{39}$	$< 3.5 \times 10^{-4}$	$< 2.3 \times 10^9$	> 7.9	< 0.3
NGC 5170	0.2 (fixed)	0.2 (fixed)	$< 7.5 \times 10^{39}$	$< 5.3 \times 10^{-4}$	$< 3.4 \times 10^9$	> 2.3	< 1.5

NOTE. — All constraints are given at 3σ significance and are derived within $r = 40$ kpc, with the D_{25} ellipses excluded. L_X is given in the 0.3–2 keV band, corrected for Galactic absorption, and $\langle \dot{M} \rangle \approx M_{\text{hot}}/\langle t_{\text{cool}} \rangle$ is the mean cool-out rate of hot gas within the assumed aperture.

cal disks, combined with the low specific star formation and supernova rates of the galaxies as discussed in § 2, suggest minimal contamination from outflows of hot gas driven beyond the optical disk of either galaxy by stellar feedback. Hence, we base our constraints on the amount of accreted hot halo gas on the net count rate limits evaluated inside the circular apertures underlying Fig. 3, i.e. a region extending to $r = 40$ kpc from immediately outside the D_{25} ellipse of each galaxy.

In order to convert observed count rate limits into constraints on the halo X-ray flux, we assume that the spectrum of any hot halo gas can be described by a thermal plasma with a given temperature, metal abundance, and volume filling factor (adopting the APEC model in XSPEC v11.3). In the absence of direct observational information on these quantities, we resort to more indirect observational constraints and to simulation results. For example, cosmological simulations predict a remarkably tight correlation between the temperature of infalling hot gas and v_c of the disk (§ 4 below; see also Toft et al. 2002), with T being in good agreement with a simple expectation for the virial temperature $T_{\text{vir}} \approx (1/2)\mu m_p v_c^2$ of the underlying dark matter halo. We therefore nominally assume $T = T_{\text{vir}} \approx 0.3$ and ≈ 0.2 keV for any halo gas around NGC 5746 and NGC 5170, respectively, based on the disk circular velocities listed in Table 1. As further justification of this choice, we note that gas much colder than T_{vir} would mainly emit at UV wavelengths and likely be subject to rapid cool-out to $T \lesssim 10^4$ K, while gas much hotter would be subject to evaporation from the galactic gravitational potential. These situations are manifestly distinct from the case of a gravitationally confined hot halo composed of infalling shock-heated material as seen in our simulations, but it is the amount and properties of any such material that is the focus of our attention.

We further note that outside the galactic disks themselves, the emission-weighted metal abundance of the X-ray gas in these simulations displays a mean and standard deviation of $Z = 0.2 \pm 0.1 Z_{\odot}$, which is consistent with observational results for the low-redshift intergalactic medium (Danforth et al. 2006), for the outskirts of groups (Rasmussen & Ponman 2007) and clusters of galaxies (e.g., Tamura et al. 2004), and for the intergalactic filaments from which these structures accrete material (Finoguenov et al. 2003). Hence, for the purpose of our spectral analysis, we here consider a fiducial value of $Z = 0.2 Z_{\odot}$ for the halo metal abundance (while noting that the *mass-weighted* abundance in the simulations is substantially lower, as discussed in § 4.3). Finally, for the volume filling factor η of hot gas, a value of unity is assumed for simplicity, since our simulations

(§ 4) indicate high values of $\eta \approx 0.8$ –1.

Using these assumptions and the appropriate ACIS-I response files, observed count rate limits were translated into corresponding constraints on the APEC plasma model normalization A ,

$$A = \frac{10^{-14}}{4\pi D^2} \int n_e n_H dV, \quad (1)$$

where D is the assumed distance (Table 1), and n_e and n_H are the number densities of electrons and hydrogen atoms, respectively. The integral represents the emission integral $I_e \equiv \int n_e n_H dV \approx \eta n_e^2 V$ of the hot halo gas inside the covered volume V . From the resulting constraint on I_e , we obtained upper limits to the mean hot gas density $\langle n_e \rangle \sim (I_e/V\eta)^{1/2} \approx (I_e/V)^{1/2}$ and total hot gas mass $M_{\text{hot}} \sim m_p \langle n_e \rangle V$ inside V . For V itself, a spherical volume of $r = 40$ kpc was assumed, with the D_{25} “cylinder” excluded along the line of sight. Using the cooling curves $\Lambda(T, Z)$ of Sutherland & Dopita (1993), we also derived constraints on the mean cooling time $\langle t_{\text{cool}} \rangle \approx 3kT/(\Lambda \langle n_e \rangle)$ and cool-out rate $\langle \dot{M} \rangle \approx M_{\text{hot}}/\langle t_{\text{cool}} \rangle$ of hot gas inside this volume.

Table 2 summarizes the derived constraints on halo properties for both galaxies, where all values have been obtained from the 3σ upper limits on the observed halo count rates using the nominal values of T , Z , and η discussed above. Note that although the two galaxies are roughly at the same distance, the combination of shorter exposure time, higher Galactic absorbing column, and assumed lower gas temperature of the NGC 5170 halo, leads to less tight constraints on the hot halo properties for this galaxy. The lower temperature is particularly important, as *Chandra* is not very sensitive to gas at $T \lesssim 0.2$ keV.

Although we have attempted to assume realistic values of T , Z , and η for the halo gas, it is worth briefly illustrating the impact of these assumptions on the derived quantities. In particular, tighter constraints would result for either galaxy if assuming a higher halo temperature or metallicity. For our best constrained case of NGC 5746, increasing both the assumed T and Z by 50% compared to the adopted values in Table 2 would reduce our upper limits on L_X and M_{hot} by roughly 30%, while doubling the lower limit on $\langle t_{\text{cool}} \rangle$. For NGC 5170, the corresponding changes would be a 40% reduction of L_X and M_{hot} , with $\langle t_{\text{cool}} \rangle$ increasing by a factor 2.8. Also note that if employing uncertainties at the 90% confidence level rather than the more conservative 3σ limits in Table 2, we would instead obtain $L_X < 2.2 (4.1) \times 10^{39} \text{ erg s}^{-1}$ and $M_{\text{hot}} = 1.7 (2.5) \times 10^9 M_{\odot}$ for NGC 5746 (NGC 5170). As will be apparent, none of these modifications would affect our overall conclusions.

4. COMPARISON TO SIMULATIONS OF GALAXY FORMATION

The lack of any detectable extraplanar hot gas related to stellar feedback is not surprising for either of our target galaxies, given the absence of any corresponding extraplanar H α or radio emission. The derived constraint on the hot halo luminosity of NGC 5746, however, is also an order of magnitude below the naive expectation from the Toft et al. (2002) simulations for cosmologically accreted gas around a galaxy of this circular velocity. Care should be exercised in directly comparing the Toft et al. (2002) predictions to our results though, as the former also include the emission from within the optical disk. Moreover, as mentioned in § 1, all the massive ($v_c \gtrsim 250 \text{ km s}^{-1}$) galaxies in the Toft et al. (2002) study were formed in the old "standard" CDM cosmology ($\Omega_m = 1$, $\Omega_\Lambda = 0$), with an assumed cosmic baryon fraction $f_b = 0.05$ or 0.10 , well below current estimates ($f_b = 0.17$; Spergel et al. 2007), and with no metal-dependence on the radiative cooling rate. The aim of this section is to explore the predictions of more sophisticated higher-resolution simulations assuming the currently prevailing Λ CDM cosmology, and test whether these can accommodate the observational constraints obtained for both our galaxies.

4.1. Cosmological Simulations

For this purpose, we have employed cosmological TreeSPH simulations of galaxy formation and evolution in a flat ($\Omega_m = 0.3$, $\Omega_\Lambda = 0.7$) Λ CDM cosmology. The code, described in detail in Sommer-Larsen et al. (2005) and Romeo et al. (2006), incorporates energetic stellar feedback in the form of starburst-driven galactic winds. Contrary to our earlier simulations used by Toft et al. (2002) to predict halo properties (as discussed in § 1 and § 2), the present simulations also incorporate self-consistent chemical evolution of the gas, including non-instantaneous recycling. They have also been evolved in time according to the entropy equation solving scheme of Springel & Hernquist (2002), rather than being based on the thermal energy equation, a modification which provides increased numerical accuracy in lower-resolution regions. In addition, the present simulations assume a cosmic baryon fraction of $f_b = 0.15$ and have all been run from an initial redshift of $z = 39$ with a mass resolution eight times higher than those described by Toft et al. (2002). At 0.5 Gyr before $z = 0$, each hot gas particle in the simulations was further split into 64 equal-mass particles to provide additional resolution of the hot gas phase, a procedure very similar to the one described by Peek et al. (2008) based on the same cosmological simulations. The final gas-phase resolution is thus 512 times that of the Toft et al. (2002) simulations, with the best resolved individual galaxies at $z = 0$ featuring a total of $\sim 1.3 \times 10^5$ hot gas particles within the central $r = 100 \text{ kpc}$, a hot gas mass resolution of $\sim 1.7 \times 10^4 M_\odot$, and an SPH smoothing length of $h_{\text{SPH}} \approx 1.5 \text{ kpc}$. As discussed by Peek et al. (2008), this resolution is sufficient to track thermal instabilities in the hot halo gas that may lead to the formation of warm ($T \sim 10^4 \text{ K}$) clouds within the ambient halo.

Although the simulation code includes stellar feedback, optionally enhanced to mimic AGN outflows, powerful

starburst-driven winds only occur in the simulations at early times ($z \gtrsim 4-5$), where they help to solve the angular momentum problem, the missing satellites problem, and possibly other problems related to the cold dark matter scenario (see, e.g., Sommer-Larsen et al. 2003). At $z \lesssim 4$, the SN II feedback is quite moderate in our simulations; for a typical $v_c = 220 \text{ km s}^{-1}$ disk galaxy, the star formation rate at $z = 0$ is $\sim 0.5 - 1 M_\odot \text{ yr}^{-1}$, comparable to the modest star formation rate of the Milky Way disk. The feedback of the individual star particles in the simulations is furthermore spatially and temporally uncorrelated (this is particularly true for SN Ia, whose mechanical, but not chemical, feedback is consequently neglected), so galactic winds do not easily develop at low redshift (see also Dahlem et al. 2006). Hence, a comparison between the simulation output at $z = 0$ and our two relatively quiescent galaxies seems justified. It is worth emphasizing that the feedback strength in the simulations is calibrated to reproduce the optical and morphological properties of observed galaxies. The X-ray emission is thus predicted without any additional adjustable parameters.

For the calculation of X-ray properties of the simulated galaxies, we followed the general procedure outlined by Toft et al. (2002). For each of the simulated galaxies at $z = 0$, a catalog of SPH gas particle positions, densities, temperatures, and masses was created. Each SPH particle was treated as an optically thin thermal plasma, and the associated X-ray luminosity calculated at the relevant position in a given photon energy band using the MEKA plasma emissivity code (Mewe et al. 1986). Total X-ray luminosities were then computed by summation over all particles in the volume of interest. The greatly increased numerical resolution of the present simulations at $z = 0$ allowed us to bypass the additional smoothing over the individual gas particles employed by Toft et al. (2002). However, as mentioned above, the increased resolution also facilitates the formation of small clouds within the hot halo via local thermal instabilities. Since the presence of such relatively dense and cold clouds may unphysically boost the X-ray output of the hot gas in its immediate vicinity (due to the local smoothing of particle properties inherent in SPH techniques), hot gas particles within h_{SPH} of "cold" ($T < 3 \times 10^4 \text{ K}$) gas were discarded from the X-ray calculations. The removed gas generally constitutes an insignificant fraction ($\lesssim 1\%$) of the total hot gas mass considered.

A few comparisons between NGC 5746 and results from an earlier version of these simulations were performed in Pedersen et al. (2006). Here we present a more detailed comparison based on the updated *Chandra* analysis of NGC 5746, while also including the results for NGC 5170 and for other, more actively star-forming, spirals as taken from the literature. Further comparisons are made to our previous results described in Toft et al. (2002), with the X-ray properties of the latter here re-calculated for the adopted aperture and energy band. However, in order to provide as fair a comparison as possible between the two simulation samples, we only consider the subset of the Toft et al. (2002) galaxies that was formed in simulations assuming the same flat ($\Omega_m = 0.3$, $\Omega_\Lambda = 0.7$) Λ CDM cosmology as adopted in our new simulations, and which assumed $f_b = 0.10$ (along with a fixed primordial chemical gas composition). Note, as mentioned

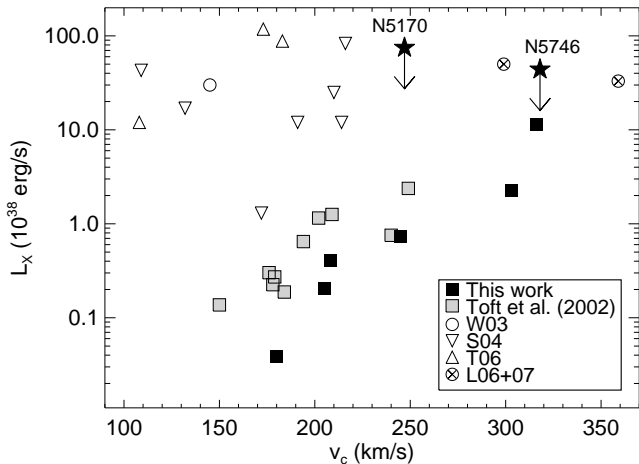


FIG. 5.— 0.3–2 keV X-ray luminosities versus v_c for our simulated galaxies (black squares), and for those of Toft et al. (2002; gray squares), all calculated assuming the NGC 5746 halo aperture. Also shown are observational results for extraplanar emission seen around other spirals, taken from Wang et al. (2003, “W03”), Strickland et al. (2004a, “S04”), Tüllmann et al. (2006a, “T06”), and Li et al. (2006, 2007, “L06+07”).

above, that this excludes all the Toft et al. (2002) galaxies with $v_c \geq 250 \text{ km s}^{-1}$, so a direct comparison of the Toft et al. results to our observed galaxies is not attempted here.

4.2. Hot Halo X-ray Luminosities

One of the hot halo properties that can be most straightforwardly compared to observations is the diffuse X-ray luminosity. For all simulated galaxies, we derived the halo L_X within the aperture also adopted for the NGC 5746 halo analysis (i.e. a spherical volume extending to $r = 40 \text{ kpc}$, with the D_{25} ellipse excluded as described in § 3.3). The results are presented in Figure 5, which shows a clear trend in hot halo L_X with galaxy mass, measured by v_c , for the simulated galaxies. Also shown are the observational constraints on the halo luminosities of NGC 5170 and NGC 5746. The simulation results are generally consistent with the constraints obtained for our observed galaxies, and we conclude that, within the adopted apertures, the lack of detectable extraplanar X-ray emission around either target agrees with these updated predictions for emission from cosmologically accreted gas.

There seems to be reasonable agreement between the results of Toft et al. (2002) and those of our newer simulations, but with a tendency towards a somewhat lower L_X at a given v_c for the latter. For example, for Milky Way-sized galaxies (v_c in the range 200–250 km s^{-1}), the mean halo luminosity for the Toft et al. (2002) galaxies is $1.4 \times 10^{38} \text{ erg s}^{-1}$, 75% higher than the corresponding result for the more recent simulations. We attribute this in part to the increased numerical resolution of the latter, as discussed in more detail later. Nevertheless, the pseudo-bolometric (0.01–10 keV) halo luminosities $L_{X,\text{bol}}$ in our new simulations remain consistent with the $L_X \propto v_c^{5-7}$ relationship found by Toft et al. (2002), with an orthogonal regression fit in $\log L_{X,\text{bol}} - \log v_c$ space yielding $L_{X,\text{bol}} \propto v_c^{5.0 \pm 0.7}$ for the new simulations. It is interesting to note that this dependence on the char-

acteristic stellar velocity of the system mirrors that of the diffuse gas in *early-type* galaxies, whose X-ray luminosity roughly obeys $L_X \propto L_B^2 \propto \sigma^{6-7}$ (based on the Faber-Jackson relation and the $L_X - L_B$ relation of O’Sullivan et al. 2001).

The amount of hot X-ray gas surrounding the galaxies in our simulations depends not only on the mass of each galaxy’s dark matter halo but also on the detailed accretion history of this halo. Numerical calculations indicate that accretion histories of galaxy-sized halos can be highly disparate even for isolated galaxies of comparable mass (e.g. van den Bosch 2002; De Rossi et al. 2008). Hence, any dependence of hot halo properties on v_c can a priori be expected to be subject to considerable scatter. Indeed, despite the clear trend in L_X with v_c for the simulated galaxies, it is important also to emphasize the considerable variation in predicted halo L_X at a given circular velocity in Fig. 5. For example, the two most massive galaxies in our new simulation sample display a factor of five variation in 0.3–2 keV L_X within the adopted aperture and yet are separated in “mass” by only $\Delta v_c = 13 \text{ km s}^{-1}$, comparable to typical observational uncertainties on v_c . This large variation at a given v_c is clearly an issue to keep in mind when comparing predicted and observed halo luminosities, or when attempting to predict hot halo fluxes for actual galaxies on the basis of simulation results.

In order to also facilitate comparison of the simulation predictions to other observational results, we have compiled available constraints from the literature on extraplanar emission seen around other spirals, although we make no claims as to the completeness of this compilation (note though that we have not included the results of Sun et al. 2007, because it is not entirely clear to what extent, if any, these spirals show *extraplanar* emission). These results are also included in Fig. 5, but we stress that the halo luminosities in these cases have not necessarily been derived within the same aperture as adopted for NGC 5746 and our simulated galaxies. For example, the results of Strickland et al. (2004a) were all derived at a distance $|z| > 2 \text{ kpc}$ from the disk midplane. If instead adopting this aperture, the increase in L_X predicted for our simulated galaxies is at the 10–40 per cent level, with no systematic dependence on v_c . We expect similar corrections for the apertures used for the additional galaxies in the Tüllmann et al. (2006a) sample, where halo X-ray properties were constrained outside the $H\alpha$ disk, again typically at $|z| > 2 \text{ kpc}$ from the midplane. These changes are relatively small, well within the scatter seen for the simulated galaxies.

The Li et al. (2006, 2007) results in Fig. 5 include unresolved emission within regions of the optical disk (though with the prominent dust lane in the Sombrero galaxy excluded; Li et al. 2007). Hence, the true halo luminosities of these galaxies should be somewhat lower than indicated in this figure, although the apertures employed by Li et al. extend to smaller radii than adopted for NGC 5746 and hence our simulated galaxies. We include these two data points in Fig. 5 for completeness, in particular because the result for the massive ($v_c \approx 359 \text{ km s}^{-1}$; HyperLeda database) Sombrero galaxy clearly poses a strong constraint on theoretical models, and since Fig. 5 suggests that the impact of its $\sim 10^9 M_\odot$ supermassive black hole on the diffuse L_X

must be rather modest. We also note that a very low halo X-ray luminosity of 3×10^{38} erg s $^{-1}$ has been reported for the $v_c \approx 250$ km s $^{-1}$ Sb spiral NGC 4565 (Wang 2005). This result would be broadly consistent with the new simulation predictions in Fig. 5 if assuming similar apertures. However, the result may be affected by emission from a nearby background cluster of galaxies (Wang 2005), and the details of the *Chandra* analysis have not been published, so we have chosen not to include this data point in Fig. 5.

Keeping the above caveats in mind, Fig. 5 indicates that the theoretical predictions can generally be accommodated by the observational results for the (presumably mainly starburst-generated) hot halos seen in other studies. The latter show X-ray luminosities for low- and intermediate-mass spirals which are up to three orders of magnitude above the simulation results at a given v_c but which are also roughly independent on v_c and show considerably larger scatter at a given v_c . It is, nevertheless, interesting that X-ray observations of high- v_c spirals (e.g., Li et al. 2007) are now providing luminosity constraints which are comparable to simulation predictions within the assumed aperture.

4.3. Halo Gas Temperatures

The inferred temperature of the hot halo gas in observations and simulations is a useful diagnostic of the nature and origin of this gas. Figure 6 shows the emission-weighted temperature $\langle T \rangle$ of hot halo gas against v_c , for all gas within the $(100 \text{ kpc})^3$ simulation volume surrounding each simulated galaxy. The predictions for the halo temperature are generally very similar to the expected virial temperature $T_{\text{vir}} \propto v_c^2$, as anticipated for accreting, shock-heated material, but with a slight tendency for $\langle T \rangle$ to mildly exceed T_{vir} . A plausible explanation for this is that our estimate of $\langle T \rangle$ is dominated by emission close to the disk, where the gas temperature rises slightly above T_{vir} , as demonstrated below. We note that a halo gas temperature slightly exceeding the virial temperature of the dark matter is also a generic feature of the phenomenological hot halo models considered by Fukugita & Peebles (2006).

In contrast to the clear T - v_c trend exhibited by the simulation sample, published temperatures for the Strickland et al. (2004a) and Li et al. (2006, 2007) samples show no obvious systematic dependence on v_c (note that single emission-weighted halo temperatures are not available for the samples of Wang et al. (2003) or Tüllmann et al. (2006a), so these galaxies are not included in this plot). Any trend with v_c for the observed galaxies must thus be subject to considerable scatter, and is possibly modulated by a dependence on additional parameters such as the star formation rate. Also note the absence of observed data points with $T \lesssim 0.2$ keV in the plot, which is at least in part related to the difficulty of detecting such low-temperature gas with *Chandra* or *XMM*. This also applies to the very low- v_c M82 — excluded here for reasons of clarity but included in Fig. 1 — for which Strickland et al. (2004a) list separate temperatures of 0.27 and 0.37 keV for the halo regions covered by ACIS-S and ACIS-I observations, respectively.

For the galaxies with detected extraplanar emission, the lack of a clear systematic trend in both L_X and T with v_c , and hence galactic mass, strongly argues against

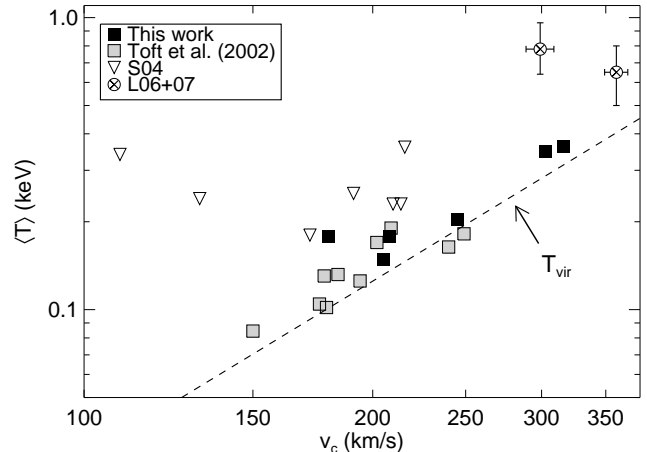


FIG. 6.— Global emission-weighted hot halo temperature versus v_c for our simulated galaxies (squares), along with observational results for extraplanar emission around other spirals, with symbols as in Fig. 5. Dashed line shows the virial estimate $T_{\text{vir}} \approx (1/2)\mu m_p v_c^2$ of the hot halo temperature.

a gravitational origin for this extraplanar emission. This interpretation gains support from the facts that the hot halo temperatures of these galaxies consistently exceed the virial temperatures expected from the circular velocity of the disk and are furthermore invariant with respect to L_X over four orders of magnitude in SFR (Grimes et al. 2005). In general, the halo gas is almost certainly related to galactic wind or fountain activity in these cases, rather than representing externally accreted material. Indeed, unambiguous kinematic evidence for outflows perpendicular to the disk has been uncovered in many of these galaxies (Strickland et al. 2004b and references therein).

A single-temperature model was assumed when constraining hot halo properties of our observed galaxies in § 3.3. To test the validity of this assumption, we investigate spatial variations in the predicted hot halo temperature in Fig. 7, in the form of emission-weighted temperature profiles extracted perpendicular to the disk. The reasonably uniform temperature distribution predicted outside the disk suggests that our assumption of a single- T model for the observed galaxies is well motivated. The one exception is the lowest- v_c galaxy, which exhibits a very prominent warp in the *cold* gas distribution that also affects the temperature distribution of its hot gas, giving rise to the abrupt change seen around $|z| \approx 25$ kpc. We note that a qualitatively very similar picture to that in Fig. 7 applies to the metal abundance of hot halo gas, once again supporting the simplifying assumption of a single hot gas phase adopted in § 3.3. This is true irrespective of considering the emission- or mass-weighted abundances, although the latter is significantly lower within the adopted aperture, with a mean and standard deviation of $Z = 0.03 \pm 0.01 Z_\odot$ compared to the corresponding emission-weighted value of $0.2 \pm 0.1 Z_\odot$.

Fig. 7 also shows that the predicted halo temperature is in good agreement with the virial temperature expected for the simulated galaxies (i.e. $T \approx 0.3$ keV for a galaxy with $v_c \approx 300$ km s $^{-1}$) at intermediate distances ($|z| \sim 20$ kpc) from the disk, but drops slightly below this value further out. The overall halo X-ray emission is dominated by gas closer to the disk, where T gen-

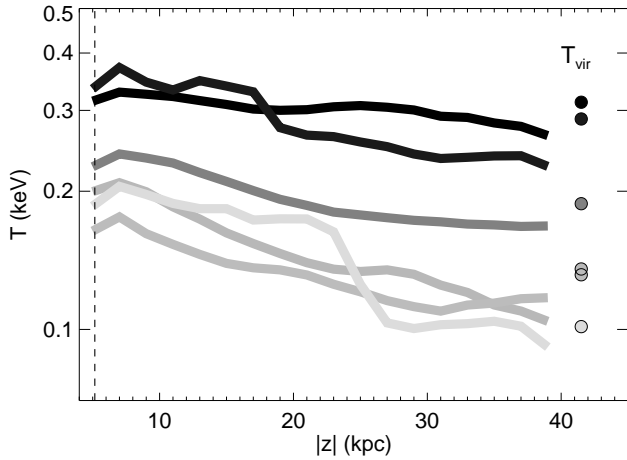


FIG. 7.— Emission-weighted temperature profiles extracted perpendicular to the disk for the simulated galaxies. The gray-scale reflects the expected virial temperature T_{vir} (darker colors indicate higher T_{vir}), with T_{vir} itself marked for each profile by a filled circle at an (arbitrary) large distance above the disk. Dashed vertical line marks the extent of the D_{25} minor axis of NGC 5746.

erally increases gently to slightly above T_{vir} , leading to the mildly super-virial global temperatures in Fig. 6. At even smaller distances from the disk midplane, the temperature shows evidence of a beginning decline as a substantial fraction of halo gas eventually reaches average densities which allow for rapid cool-out. This is reminiscent of a classical central cooling flow, but it is worth emphasizing that cool-out of halo gas in these simulations also proceeds via condensation of small pressure-supported clouds at various distances from the disk, with a monotonic increase in overall mass cool-out rate with decreasing galactocentric distance (Sommer-Larsen 2006; Peek et al. 2008). Also note that although some gas is thus cooling rapidly in the central halo regions, Fig. 7 still suggests that the X-ray gas outside the disk could appear near-isothermal. This behavior could potentially compromise direct observational tests of whether halo gas is indeed cooling to below X-ray temperatures (e.g. via X-ray grating spectroscopy), as much of the cooling occurs very close to the optical disk where absorption by cold gas and contamination from other X-ray sources, diffuse and point-like, could be substantial.

4.4. Hot Gas Mass and Cool-Out Rates

In the context of understanding the “missing baryon” problem in disk galaxies (e.g. Maller & Bullock 2004; Fukugita & Peebles 2006; Sommer-Larsen 2006), the total amount of hot halo gas around such galaxies is a crucial quantity. For our simulations, the correlation between hot gas mass M_{hot} within the NGC 5746 aperture and v_c is displayed in Fig. 8a. Given that the simulations also include cold, non-X-ray emitting gas around the galaxies and that M_{hot} is not an X-ray emission-weighted quantity, a low-temperature cut at $T = 0.05$ keV was imposed on the simulated galaxies in order to provide a sensible comparison to the *Chandra* constraints on X-ray emitting gas mass. This temperature cut is well below T_{vir} for all the simulated galaxies (cf. Fig. 6), and is probably close to the lower limit at which gas can be reliably detected in emission in typical *Chandra*

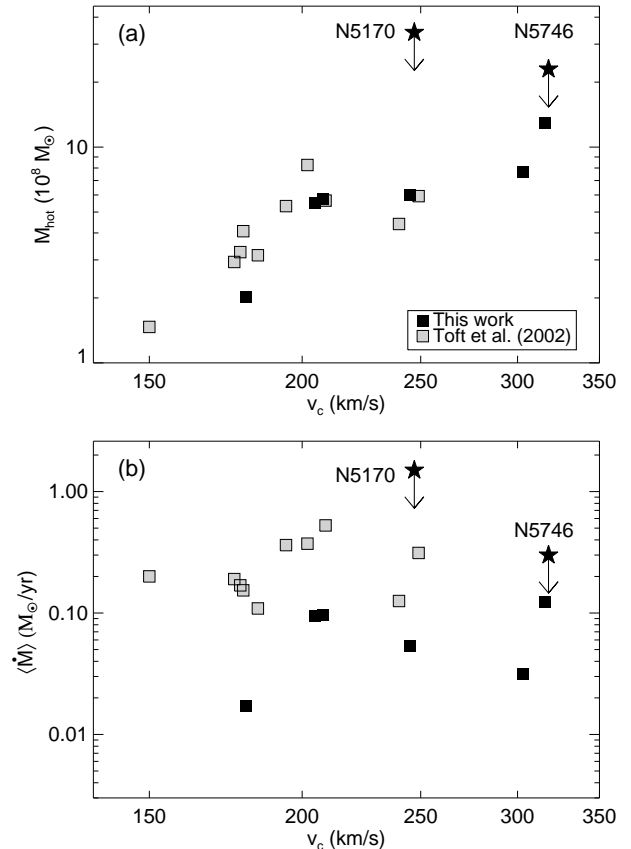


FIG. 8.— (a) Mass of hot ($T \geq 0.05$ keV) gas as a function of v_c within the NGC 5746 halo aperture, with symbols as in Fig. 5. (b) The corresponding mean hot gas cool-out rate, $\langle \dot{M} \rangle \approx M_{\text{gas}} / \langle t_{\text{cool}} \rangle$.

or *XMM* exposures (see, for example, the discussion in Rasmussen et al. 2004b).

As anticipated, a clear trend with v_c is present for the simulation results. These are also seen to be consistent with our observational constraints, but we note that the 3σ upper limit derived for NGC 5746 is here only within a factor of 2–3 of the simulation predictions for a galaxy of this mass. Clearly, any changes in the assumed input physics in the simulations that would result in significantly higher hot halo masses at $z = 0$ are disfavored by our observations. Also note that the overall hot gas masses within this aperture at a given $v_c \gtrsim 200$ km s $^{-1}$ are similar for the two simulation samples, despite the clear differences in corresponding L_X visible in Fig. 5. The main explanation is that the increased numerical resolution employed here, and the removal of a small amount of hot gas particles within an SPH smoothing length of cold gas in the new simulations, reduces the amount of (artificially) strongly X-ray emitting high-density halo gas.

The predicted amount of hot halo gas within the adopted aperture is $M_{\text{hot}} \lesssim 10^9 M_{\odot}$ for Milky Way-sized galaxies, corresponding to only $\lesssim 2\%$ of the baryonic disk mass of such galaxies. The situation for our observed galaxies is unlikely to be significantly different. In fact, Rand & Benjamin (2008) used the inferred HI rotation curve of NGC 5746 to derive a dynamical mass

inside $r \approx 40$ kpc of $7.9 \times 10^{11} M_{\odot}$, which, combined with M_{hot} from Table 2, implies that any hot halo gas outside the optical disk contributes less than 0.3% of the total mass budget within this radius. In terms of baryonic mass, the inferred HI mass in the disk of $1 \times 10^{10} M_{\odot}$, added to a stellar mass of $1.6 \times 10^{11} M_{\odot}$ as estimated from the optical parameters in Table 1 using the prescription of Mannucci et al. (2005), implies that $\lesssim 1\%$ of the baryons in NGC 5746 are in a hot phase within $r = 40$ kpc. For NGC 5170, the corresponding constraint is $\lesssim 4\%$, based on a stellar mass of $6 \times 10^{10} M_{\odot}$ and an HI mass of $1.4 \times 10^{10} M_{\odot}$ (Bottema et al. 1987).

These fractions are expected to grow drastically with galactocentric distance, however, as most of the diffuse hot baryons associated with our simulated galaxies reside beyond the $r = 40$ kpc aperture probed here. As discussed in detail in Sommer-Larsen (2006), the total mass of hot halo gas within the virial radius may equal or exceed the mass of cold baryons in the disk of a simulated $v_c \approx 300$ km s $^{-1}$ galaxy. For our observed galaxies, this possibility is still allowed by our constraints in Figure 8, provided that the radial distribution of any hot halo gas around our galaxies is not significantly steeper than in these simulations. Deeper X-ray observations would be required to test this scenario in detail, but observational verification of this prediction would clearly help in resolving the well-known “missing baryon” problem in disk galaxies.

As a final comparison between the simulations and our observational constraints, Fig. 8b shows the results for the mean cool-out rate $\langle \dot{M} \rangle \approx M_{\text{hot}} / \langle t_{\text{cool}} \rangle$ of hot gas within the NGC 5746 aperture. Again, a temperature cut at $T = 0.05$ keV was imposed on the simulations, but \dot{M} was otherwise estimated in the same manner as for the observed galaxies (§ 3.3), i.e. with hot gas cooling times $\langle t_{\text{cool}} \rangle$ derived assuming the metal-dependent cooling curves $\Lambda(T, Z)$ of Sutherland & Dopita (1993). The figure reveals substantial scatter at any given v_c and no clear systematic variation with this quantity. The simulation predictions again remain consistent with our observational results as listed in Table 2. The difference between the Toft et al. (2002) and newer simulations is largely due to lower mean cooling times for the hot gas in the former, for the reason discussed above.

It is important to note, however, that the estimated values of \dot{M} should not be identified with the actual accretion rate of hot halo gas onto the disk, in part because these estimates do not include the gas condensing out of the hot halo phase due to small-scale thermal instabilities (see, e.g. Peek et al. 2008), but more importantly because our \dot{M} does not take into account the gas cooling *inside* the inner boundary of the adopted aperture. In practice, the derived values of \dot{M} should be considered lower limits to the true disk accretion rates in the simulations. For a detailed discussion of actual accretion rates for the simulated galaxies, we refer to Sommer-Larsen et al. (2003) and Peek et al. (2008). Such a discussion is beyond the scope of this work, also because it is not straightforward to compare these rates to our observational constraints in Table 2.

5. DISCUSSION

We emphasize that the observational part of this study was initiated on the basis of the predictions of Toft et al. (2002), which suggested that the performed observations of NGC 5746 would be sufficiently sensitive to reveal the presence of an accreted hot halo. Our newer simulations predict somewhat lower hot halo luminosities outside the disk, in consistency with the inferred absence of detectable hot halo gas around both NGC 5746 and NGC 5170. It is nevertheless clear that observational results for massive galaxies are within factors of a few of the theoretical predictions for halo luminosity and gas mass, and can potentially begin to test the input physics in cosmological simulations. For example, the predicted hot gas mass for $v_c \approx 300$ km s $^{-1}$ galaxies is within a factor of 2–3 of the upper limit derived for NGC 5746. Numerical effects aside, inferred halo X-ray luminosities of even more massive galaxies such as NGC 4594 (cf. Fig. 5) clearly leave limited scope for changes in the simulation input physics that would raise the predicted present-day halo L_X , though with the caveat that the simulations show some “cosmic variance” at a given v_c . Further high-sensitivity observations may begin to seriously challenge the theoretical models and provide useful constraints on, for example, the galactic feedback prescriptions implemented in state-of-the-art numerical work.

Compared to the earlier results presented by Toft et al. (2002), it is also clear that the X-ray luminosity and cool-out rate of hot halo gas are somewhat lower in the more recent simulations. One possible reason is the higher mass resolution of the latter, which helps to suppress the importance of a problem associated with the spatial smoothing inherent in SPH techniques, namely the possibility that the properties of hot gas particles can become strongly affected by those of much colder and denser particles in their immediate vicinity. As a rough test of the impact of improving the hot gas mass resolution, we re-simulated our lowest-mass ($v_c \approx 180$ km s $^{-1}$) galaxy from $z = 39$ at 64 times the Toft et al. (2002) resolution, with each hot gas particle then subsequently split into eight equal-mass ones at a later stage. At high z , this version is thus eight times better resolved than the one shown in Fig. 5, and the halo L_X is here found to be 50% lower. An additional test for a more massive galaxy, the $z \approx 1$ version of the $v_c \approx 245$ km s $^{-1}$ disk in Fig. 5, showed little change in halo L_X at higher resolution, however. This suggests that higher resolution may decrease the predicted L_X somewhat, but the reduction is moderate (well within the factor 4–5 in “cosmic variance” that is evident in Fig. 5), and L_X may be close to convergence at the high-mass end. We do not currently have higher-resolution versions of our most massive galaxies at $z = 0$ due to the prohibitive CPU times required, so more detailed tests of the impact of numerical resolution will remain the subject of future work.

Two other effects also act to reduce the present-day hot halo luminosity in the updated simulations, namely the higher assumed cosmic baryon fraction $f_b = 0.15$ (vs. $f_b = 0.10$ for the comparison galaxies of Toft et al. 2002 considered here) and the higher metal abundance resulting from implementing chemical evolution in the simulation code. This may at first seem counter-intuitive, but the increased radiative cooling efficiency implied by both these modifications actually results in less hot and dense gas remaining in the halo at $z = 0$ for a given v_c

(see also Rasmussen et al. 2004a; Sommer-Larsen 2006). Note that both the hot gas fraction and the total “external” (non-disk) baryon fraction inside the virial radius are reduced at fixed v_c when assuming higher f_b , not only because the accreted shock-heated gas can leave the X-ray phase more rapidly, but also because the virial radius itself decreases at a given v_c as a consequence (Sommer-Larsen 2006).

Despite the reduced X-ray output in the current simulations, we readily acknowledge the points raised by Li et al. (2006, 2007) and Wang (2007). Their comparison of observational results obtained for NGC 2613 and NGC 4594 to the 0.2–2 keV luminosities of Toft et al. (2002) indicate that the latter overpredict total (disk plus halo) intrinsic X-ray luminosities by at least a factor of 10 for these massive galaxies. This discrepancy is at least in part related to the common over-cooling problem in hydrodynamical simulations, a problem which also plagues the current simulations at some level (Romeo et al. 2006). However, driven by the requirement to avoid confusing any halo emission with emission produced by unrelated processes, we have to some extent circumvented that issue here by only considering the X-ray properties of gas outside the optical disk. Note also that both the Toft et al. (2002) and present simulations do not incorporate the effects of intrinsic X-ray absorption by cold gas and dust in the disk, which can naturally be substantial for edge-on galaxies and may be non-trivial to properly correct for across the full optical extent of the galaxy in observational studies.

While our results suggest that increased numerical resolution may help to alleviate the issue of over-cooling somewhat, it is also possible, as hypothesized by Li et al. (2006, 2007), that some over-cooling in the simulations is related to incomplete treatment of feedback from SN Ia, if these can provide large-scale distributed heating. As mentioned, *mechanical* feedback from SN Ia is not included in the present simulations, but Wang (2007) suggest that numerous SN Ia in early-type spirals (such as NGC 2613, 4594, and 5746) could generate a bulge wind which would be sufficiently powerful to suppress the cooling of any infalling halo material and lower its X-ray luminosity. Observational verification of the presence of SN Ia-driven winds in spirals would certainly provide an important new ingredient to be incorporated in numerical simulations. Our X-ray data of NGC 5746 and NGC 5170 do not allow a direct observational test of this scenario, apart from requiring such outflows to have X-ray luminosities below the inferred halo upper limits. The discussion pertaining to Fig. 1, although based on somewhat simplistic assumptions, suggests that direct supernova blow-out of disk material is unlikely to be important in our two galaxies even if including SN Ia. Our galaxies may therefore not represent optimal targets for an observational test of this scenario.

Wang (2007) also proposes another possible solution to the over-cooling problem, noting that the halo gas may be chemically inhomogeneous but generally very low in metallicity. While metal-rich clouds can cool out rapidly and fall towards the disk, most of the halo gas may thus radiate inefficiently and would be difficult to detect in either emission or absorption. Although an interesting possibility, it is not obvious that this explanation may necessarily help to solve the over-cooling problem. As

discussed above, the metal-free halos in the Toft et al. (2002) simulations are actually *more* X-ray luminous at a given v_c at zero redshift than those in our more recent simulations. Other factors such as the assumed cosmic f_b in the simulations may play a role for this result, as already mentioned, but this difference between metal-enriched and metal-free halos persists even when considering halos in simulations run with identical cosmological parameters and numerical resolution (Rasmussen et al. 2004a). Allowing for chemical enrichment in our simulations systematically reduces the predicted present-day halo luminosity for a given v_c .

On the observational front, it is generally well established that disk galaxies have experienced considerable stellar mass growth since $z \approx 1$ (e.g. Barden et al. 2005 and references therein), and both observational and theoretical evidence suggests that gas consumption, rather than major merger activity, has played the dominant role in driving this growth (de Ravel et al. 2008; De Rossi et al. 2008; Daddi et al. 2008). The hot halos discussed in this paper could potentially have supplied most of the fuel required for the continued growth of disks, provided that cool-out of such gas is not strongly inhibited by, for example, disk feedback processes. Despite the absence of a detectable large-scale X-ray corona around either of our target galaxies, hot coronal gas surrounding both targets could still be present below our detection limits. It remains unclear, however, to what extent any such gas is currently cooling out to replenish the gas consumed by star formation in their disks, and if so, whether this proceeds mainly as a central cooling flow or through condensation and infall of small clouds across a wide range of galactocentric distances within a hot halo. For NGC 5746, our naive constraint on the cool-out rate of hot halo gas outside the optical disk, $\dot{M} < 0.3 M_\odot \text{ yr}^{-1}$, suggests that large-scale cooling from a hot halo cannot balance the SFR in the disk of $0.9 \pm 0.2 M_\odot \text{ yr}^{-1}$. It is important to reiterate, however, that the estimated cooling rates should be considered lower limits to the total rate at which halo gas may leave the hot phase and accrete onto the disk (§ 4.4), so our results are not necessarily inconsistent with the possibility that a hot halo around NGC 5746 can supply the disk with material at rates comparable to the SFR. For NGC 5170, the weaker upper limit on \dot{M} is a factor of ~ 3 above the inferred SFR, again precluding any definitive conclusions in this regard.

As suggested by a number of theoretical models, and, indeed, by the simulations presented here (see Peek et al. 2008), local thermal instabilities within a hot halo can also produce small pressure-supported clouds that would fall towards the disk on time-scales well below the cooling time of the ambient hot gas. This would contribute to feeding ongoing star formation and could potentially represent the dominant accretion mode for Milky Way-sized spirals (Maller & Bullock 2004). However, HI observations of nearby spirals generally suggest that infall of cold gas does not occur at rates sufficient to sustain star formation in the disk (Sancisi et al. 2008). Hence, infall of additional, possibly hot, material (at an average rate of $\approx 1 M_\odot \text{ yr}^{-1}$) seems required to balance gas consumption by star formation, in line with the findings of Peek et al. (2008). Of particular relevance here is the

study of Rand & Benjamin (2008), who searched for evidence of an extended HI component around NGC 5746 associated with infalling cold clouds. While the presence of vertically extended HI was detected, the majority of this gas is best interpreted as a warp rather than as an extended HI halo such as has been reported around a number of other nearby spirals (Fraternali & Binney 2006). A number of high- $|z|$ neutral clouds were also seen, possibly representing infalling material, though association with a disk-halo flow cannot be excluded for most of these. No corresponding study has, to our knowledge, been conducted for NGC 5170.

Thus, given the present data, it remains debatable whether the current SFR in galaxies such as NGC 5746 can be balanced by infall of halo material. Cold gas accretion alone seems insufficient both in NGC 5746 and in other nearby spirals, and our upper limit on the hot gas infall rate does not include gas cooling out within the disk region itself, so the interpretation of the observational X-ray results is not straightforward. It is apparent, however, that cooling of hot halo gas outside the optical D_{25} ellipse may not be able to balance star formation in NGC 5746. Interestingly, Fraternali & Binney (2008) offer a different accretion scenario that may reconcile the discrepant accretion and SFR estimates in nearby spirals without invoking substantial direct cool-out of hot halo material. In their model, accretion has an important contribution from supernova-ejected fountain clouds which sweep up (hot or cold) ambient halo gas before returning to the disk, losing angular momentum in the process. Their combined fountain plus accretion models provide a better match to the extraplanar HI velocity distribution in a few well-studied edge-on spirals than a fountain model alone, and yield accretion rates comparable to the SFR in these galaxies. Direct observational verification of this scenario may prove difficult, however, and cosmological simulations still lack the resolution to adequately capture such processes.

6. SUMMARY AND CONCLUSIONS

We have used X-ray data to re-visit our earlier claimed detection (Pedersen et al. 2006) of a large-scale diffuse X-ray halo surrounding the massive edge-on spiral NGC 5746. An analogous analysis of the less massive NGC 5170 has been completed for comparison. Our updated *Chandra* analysis employs calibration data which accounts for the positional dependence of the contaminant on the *Chandra* optical blocking filters (unlike the Pedersen et al. 2006 analysis, which could not take this into account), and has failed to reveal a statistically significant detection of extraplanar X-ray emission around either galaxy. We find that both the spatial and spectral hot halo properties of NGC 5746 as reported by Pedersen et al. (2006) are consistent with being due to the spatial variation of the degradation in the ACIS CCD quantum efficiencies.

Both our target galaxies show no signs of significant nuclear or star formation activity. This is supported by our H α imaging of both galaxies and by radio data taken from the literature, suggesting that the constraints on extraplanar X-ray emission obtained for both galaxies can be used to also place constraints on the properties of intergalactic, shock-heated material accreting onto their disks as predicted by disk galaxy formation

models and cosmological hydro-simulations. If assuming halo gas close to the expected virial temperature as suggested by such theoretical work, we constrain the total 0.3–2 keV luminosity of the halos within $r = 40$ kpc from the optical disk to $L_X < 4.0 \times 10^{39}$ (NGC 5746) and $< 7.5 \times 10^{39}$ erg s $^{-1}$ (NGC 5170) at 3σ significance. The corresponding hot gas masses are $M_{\text{hot}} < 2.3 \times 10^9$ and $< 3.4 \times 10^9 M_\odot$, respectively.

We have performed a detailed comparison of these constraints to results of recent cosmological simulations of galaxy formation and evolution. These simulations represent an update of our earlier work in Toft et al. (2002), and predict hot halo luminosities and gas masses which are consistent with the limits obtained for both NGC 5746 and NGC 5170. Outside the optical disk, the simulations show hot halo luminosities which are somewhat lower than the Toft et al. (2002) results, specifically by a factor of two for Milky Way-sized galaxies, mainly due to increased numerical resolution, the assumption of a higher baryon fraction, and the inclusion of chemical feedback. We find that “cosmic variance” in simulated halo properties can be quite substantial, with halo L_X potentially varying by a factor 4–5 for galaxies of comparable mass as measured by their disk circular velocity v_c .

Published results for all other galaxies with detected extraplanar emission can generally accommodate our simulation predictions, but observational results for high-mass spirals are clearly providing strong constraints on theoretical models for disk galaxy evolution. Based on the inferred halo temperatures and luminosities, we confirm that the hot halo emission so far observed around other spirals is in general predominantly related to activity in the disk rather than being caused by infalling, externally accreted material.

An unambiguous detection of externally accreted X-ray emitting gas around spirals is still pending. Deeper X-ray observations of carefully selected targets are required to detect such halos, but, encouragingly, our simulations suggest that this remains within reach of current X-ray instrumentation. Based on a rather modest *Chandra* exposure of less than 40 ks, we have constrained an X-ray luminosity and hot gas mass around NGC 5746 which are both within a factor of a few of the simulation predictions for a galaxy of this mass. Other existing observational constraints (e.g., Li et al. 2007) are also close to the theoretical results and can potentially begin to test the assumed input physics in numerical simulations of galaxy formation and evolution.

We thank the referee for useful comments that improved the clarity of this paper. This work has made use of the HyperLeda, NASA/IPAC (NED), and Two Micron All Sky Survey (2MASS) extragalactic databases, and was supported by the DFG Cluster of Excellence “Origin and Structure of the Universe”. JR acknowledges support provided by the National Aeronautics and Space Administration through Chandra Postdoctoral Fellowship Award Number PF7-80050 issued by the Chandra X-ray Observatory Center, which is operated by the Smithsonian Astrophysical Observatory for and on behalf of the National Aeronautics and Space Administration under contract NAS8-03060. KP acknowledges sup-

port from Instrument Center for Danish Astrophysics. We gratefully acknowledge abundant access to the computing facilities provided by the Danish Centre for Scientific Computing (DCSC), with which all computations re-

ported in this paper were performed. The Dark Cosmology Centre is funded by the Danish National Research Foundation.

REFERENCES

- Balogh, M. L., Pearce, F. R., Bower, R. G., & Kay, S. T. 2001, *MNRAS*, 326, 1228
- Barden, M., et al. 2005, *ApJ*, 635, 959
- Bendo, G. J., et al. 2006, *ApJ*, 645, 134
- Benson, A. J., Bower, R. G., Frenk, C. S., & White, S. D. M. 2000, *MNRAS*, 314, 557
- Bertin, E., & Arnouts, S. 1996, *A&AS*, 117, 393
- Binney, J. 1977, *ApJ*, 215, 483
- Binney, J. 2004, *MNRAS*, 347, 1093
- Birnboim, Y., & Dekel, A. 2003, *MNRAS*, 345, 349
- Bottema, R., van der Kruit, P. C., & Freeman, K. C. 1987, *A&A*, 178, 77
- Bower, R. G., Benson, A. J., Malbon, R., Helly, J. C., Frenk, C. S., Baugh, C. M., Cole, S., & Lacey, C. G. 2006, *MNRAS*, 370, 645
- Bregman, J. N., & Lloyd-Davies, E. J. 2007, *ApJ*, 669, 990
- Casuso, E., & Beckman, J. E. 2004, *A&A*, 419, 181
- Cen, R., & Ostriker, J. P. 1999, *ApJ*, 514, 1
- Cole, S., Lacey, C. G., Baugh, C. M., & Frenk, C. S. 2000, *MNRAS*, 319, 168
- Collins, J. A., Shull, J. M., & Giroux, M. L. 2007, *ApJ*, 657, 271
- Condon, J. J., Cotton, W. D., Greisen, E. W., Yin, Q. F., Perley, R. A., Taylor, G. B., & Broderick, J. J. 1998, *AJ*, 115, 1693
- Croton, D. J., et al. 2006, *MNRAS*, 365, 11
- Daddi, E., Dannerbauer, H., Elbaz, D., Dickinson, M., Morrison, G., Stern, D., & Ravindranath, S. 2008, *ApJ*, 673, L21
- Dahlem, M., Lisenfeld, U., & Rossa, J. 2006, *A&A*, 457, 121
- Danforth, C. W., Shull, J. M., Rosenberg, J. L., & Stocke, J. T. 2006, *ApJ*, 640, 716
- Davé, R., et al. 2001, *ApJ*, 552, 473
- Dekel, A., & Birnboim, Y. 2006, *MNRAS*, 368, 2
- de Ravel, L., et al. 2008, *A&A*, in press (arXiv:0807.2578)
- De Rossi, M. E., Tissera, P. B., De Lucia, G., & Kauffmann, G. 2008, *MNRAS*, in press (arXiv:0806.2872)
- Dickey, J. M., & Lockman, F. J. 1990, *ARA&A*, 28, 215
- Ehle, M. 2004, in *ASP Conf. Ser. 331, Extra-Planar Gas*, ed. R. Braun (San Francisco: ASP), 337
- Fabbiano, G., & Juda, J. Z. 1997, *ApJ*, 476, 666
- Finoguenov, A., Briel, U. G., & Henry, J. P. 2003, *A&A*, 410, 777
- Fraternali, F., & Binney, J. J. 2006, *MNRAS*, 366, 449
- Fraternali, F., & Binney, J. J. 2008, *MNRAS*, 386, 935
- Fukugita, M., & Peebles, P. J. E. 2006, *ApJ*, 639, 590
- Governato, F., et al. 2004, *ApJ*, 607, 688
- Grimes, J. P., Heckman, T., Strickland, D., & Ptak, A. 2005, *ApJ*, 628, 187
- Hatton, S., Devriendt, J. E. G., Ninin, S., Bouchet, F. R., Guiderdoni, B., & Vibert, D. 2003, *MNRAS*, 343, 75
- Kaufmann, T., Mayer, L., Wadsley, J., Stadel, J., & Moore, B. 2006, *MNRAS*, 370, 1612
- Kennicutt, R. C., Jr. 1998, *ApJ*, 498, 541
- Kereš, D., Katz, N., Weinberg, D. H., & Davé, R. 2005, *MNRAS*, 363, 2
- Kregel, M., van der Kruit, P. C., & de Blok, W. J. G. 2004, *MNRAS*, 352, 768
- Li, Z., Wang, Q. D., & Hameed, S. 2007, *MNRAS*, 376, 960
- Li, Z., Wang, Q. D., Irwin, J. A., & Chaves, T. 2006, *MNRAS*, 371, 147
- Maller, A. H., & Bullock, J. S. 2004, *MNRAS*, 355, 694
- Mannucci, F., della Valle, M., Panagia, N., Cappellaro, E., Cresci, G., Maiolino, R., Petrosian, A., & Turatto, M. 2005, *A&A*, 433, 807
- Mewe, R., Lemen, J. R., & van den Oord, G. H. J. 1986, *A&AS*, 65, 511
- Moshir, M., et al. 1990, *IRAS Faint Source Catalogue*, version 2.0 (1990)
- Moore, B., & Davis, M. 1994, *MNRAS*, 270, 209
- Nicastro, F., et al. 2005, *Nature*, 433, 495
- Nilsson, K. K., Fynbo, J. P. U., Møller, P., Sommer-Larsen, J., & Ledoux, C. 2006, *A&A*, 452, L23
- O'Sullivan, E., Forbes, D. A., & Ponman, T. J. 2001, *MNRAS*, 328, 461
- Pedersen, K., Rasmussen, J., Sommer-Larsen, J., Toft, S., Benson, A., & Bower, R. G. 2006, *New Astronomy*, 11, 465
- Peek, J. E. G., Putman, M. E., & Sommer-Larsen, J. 2008, *ApJ*, 674, 227
- Quilis, V., & Moore, B. 2001, *ApJ*, 555, L95
- Rand, R. J., & Benjamin, R. A. 2008, *ApJ*, 676, 991
- Rasmussen, J., Ponman, T. J., 2007, *MNRAS*, 380, 1554
- Rasmussen, J., Ponman, T. J., & Mulchaey, J. S. 2006, *MNRAS*, 370, 453
- Rasmussen, J., Sommer-Larsen, J., Toft, S., & Pedersen, K. 2004a, *MNRAS*, 349, 255
- Rasmussen, J., Stevens, I. R., & Ponman, T. J. 2004b, *MNRAS*, 354, 259
- Read, A. M., & Ponman, T. J. 2001, *MNRAS*, 328, 127
- Rice, W., Lonsdale, C. J., Soifer, B. T., Neugebauer, G., Koplan, E. L., Lloyd, L. A., de Jong, T., & Habing, H. J. 1988, *ApJS*, 68, 91
- Romeo, A. D., Sommer-Larsen, J., Portinari, L., & Antonuccio-Delogu, V. 2006, *MNRAS*, 371, 548
- Rossa, J., & Dettmar, R.-J. 2000, *A&A*, 359, 433
- Sancisi, R., Fraternali, F., Oosterloo, T., & van der Hulst, T. 2008, *A&A Rev.*, 15, 189
- Sanders, D. B., Mazzarella, J. M., Kim, D.-C., Surace, J. A., & Soifer, B. T. 2003, *AJ*, 126, 1607
- Sanders, D. B., & Mirabel, I. F. 1996, *ARA&A*, 34, 749
- Savage, B. D., Lehner, N., Wakker, B. P., Sembach, K. R., & Tripp, T. M. 2005, *ApJ*, 626, 776
- Sembach, K. R., et al. 2003, *ApJS*, 146, 165
- Smith, D. J. B., Jarvis, M. J., Lacy, M., & Martínez-Sansigre, A. 2008, *MNRAS*, 389, 799
- Softan, A. M. 2006, *A&A*, 460, 59
- Sommer-Larsen, J. 2006, *ApJ*, 644, L1
- Sommer-Larsen, J., & Dolgov, A. 2001, *ApJ*, 551, 608
- Sommer-Larsen, J., Götz, M., & Portinari, L. 2003, *ApJ*, 596, 47
- Sommer-Larsen, J., Romeo, A., & Portinari, L. 2005, *MNRAS*, 357, 478
- Spergel, D. N., et al. 2007, *ApJS*, 170, 377
- Strickland, D. K., & Heckman, T. M. 2002, *MNRAS*, 333, 649
- Strickland, D. K., Heckman, T. M., Colbert, E. J. M., Hoopes, C. G., & Weaver, K. A. 2004a, *ApJS*, 151, 193
- Strickland, D. K., Heckman, T. M., Colbert, E. J. M., Hoopes, C. G., & Weaver, K. A. 2004b, *ApJ*, 606, 829
- Sun, M., Jones, C., Forman, W., Vikhlinin, A., Donahue, M., & Voit, M. 2007, *ApJ*, 657, 197
- Sutherland, R. S., & Dopita, M. A. 1993, *ApJS*, 88, 253
- Tamura, T., Kaastra, J. S., den Herder, J. W. A., Bleeker, J. A. M., & Peterson, J. R. 2004, *A&A*, 420, 135
- Temple, R. F., Raychaudhury, S., & Stevens, I. R. 2005, *MNRAS*, 362, 581
- Toft, S., Rasmussen, J., Sommer-Larsen, J., & Pedersen, K. 2002, *MNRAS*, 335, 799
- Tripp, T. M., Savage, B. D., & Jenkins, E. B. 2000, *ApJ*, 534, L1
- Tüllmann, R., Pietsch, W., Rossa, J., Breitschwerdt, D., & Dettmar, R.-J., 2006a, *A&A*, 448, 43
- Tüllmann, R., Breitschwerdt, D., Rossa, J., Pietsch, W., & Dettmar, R.-J. 2006b, *A&A*, 457, 779
- van den Bosch, F. C. 2002, *MNRAS*, 331, 98
- van der Hulst, T., & Sancisi, R. 2004, in *ASP Conf. Ser. 331, Extra-Planar Gas*, ed. R. Braun (San Francisco: ASP), 139
- Wakker, B. P., et al. 1999, *Nature*, 402, 388
- Wang, Q. D. 2005, in *ASP Conf. Ser. 331, Extra-Planar Gas*, ed. R. Braun (San Francisco: ASP), 329
- Wang, Q. D. 2007, *EAS*, 24, 59
- Wang, Q. D., Chaves, T., & Irwin, J. A. 2003, *ApJ*, 598, 969
- Wang, Q. D., Immler, S., Walterbos, R., Lauroesch, J. T., & Breitschwerdt, D. 2001, *ApJ*, 555, L99
- White, S. D. M., & Frenk, C. S. 1991, *ApJ*, 379, 52
- White, S. D. M., & Rees, M. J. 1978, *MNRAS*, 183, 341